A comparative study between human skin substitutes and normal human skin using Raman microspectroscopy

Marie Leroy[a,b,c,d], Jean-François Labbé[d], Marise Ouellet[d], Jessica Jean[c], Thierry Lefèvre[d], Gaétan Laroche[a,b], Michèle Auger[d*] and Roxane Pouliot[c*]

[a]*Laboratoire d'Ingénierie de Surface (LIS), Département de Génie des Mines, de la Métallurgie et des Matériaux, Centre de Recherche sur les Matériaux Avancés (CERMA), Université Laval, 1065 avenue de la médecine, Québec (QC), Canada, G1V 0A6.*
[b]*Centre de Recherche du Centre Hospitalier Universitaire de Québec (CRCHUQ), Hôpital St-François d'Assise, 10 rue de l'Espinay, Québec (QC), Canada, G1L 3L5.*
[c]*Centre LOEX de l'Université Laval, Génie Tissulaire et Régénération: LOEX-Centre de Recherche du Centre Hospitalier Universitaire de Québec (QC), Hôpital de l'Enfant Jesus, 1401, 18e rue, Québec (QC). Canada, G1J 1Z4.*
[d]*Département de Chimie, Regroupement québécois sur la fonction, la structure et l'ingénierie des protéines (PROTEO), CERMA, Université Laval, 1045 avenue de la médecine, Québec (QC), Canada, G1V 0A6.*

ABSTRACT
Research in the field of bioengineered skin substitutes is motivated by the need to find new dressings for people affected by skin injuries (burns, diabetic ulcers), and to develop adequate skin models to test new formulations developed in vitro. Thanks to advances in tissue engineering, it is now possible to produce human skin substitutes, without any exogenous material, using the self-assembly method developed by the LOEX (Laboratoire d'Oganogénèse Expérimentale). These human skin substitutes consist of a dermis and a stratified epidermis (stratum corneum and living epidermis). Raman microspectroscopy has been used to characterize and compare the molecular organization of skin substitutes with normal human skin. Our results confirm that the stratum corneum is a layer rich in lipids which are well-ordered (trans conformers) in both substitutes and normal human skin. The amount of lipids decreases, and more gauche conformers appear in the living epidermis, in both cases. However, the results also show that there are fewer lipids in the substitutes and that the lipids are more organized in the normal human skin. Concerning the secondary structure of proteins and protein content, the data show that they are similar in the substitutes and in normal human skin. In fact, the epidermis is rich in α-keratin, whereas the dermis contains mainly type I collagen.

KEYWORDS
Human skin substitutes, lipid organization, protein structure, Raman microspectroscopy

CITATION
Leroy, M., Labbé, J. F., Ouellet, M., Jean, J., Lefèvre, T., Laroche, G., ... & Pouliot, R. (2014). A comparative study between human skin substitutes and normal human skin using Raman microspectroscopy. Acta biomaterialia, 10(6), 2703-2711.

1 INTRODUCTION

According to the World Health Organization, burns are a global public health problem, accounting for an estimated 195,000 deaths annually. In 2008, over 410,000 burn injuries occurred in the United States of America, with approximately 40,000 requiring hospitalization [1]. Wound healing can be problematic not only in the case of large burns, but also in the case of chronic wound (diabetic ulcers). From a dermo-pharmacological point of view, there is a need of skin models to test new formulations developed in vitro. Concerning cosmetic products, a new legislation in Europe, which is effective since July 2013, specifies that animal testing must be replaced by alternative methods. Moreover, this regulation also applies to all products to be distributed throughout the European market and has therefore consequences for the cosmetic industry all over the world [2]. In this context, there is a high need for human skin substitutes (HSS). In fact, the use of autologous skin substitutes seems to be the best treatment for chronic wounds and the treatment of deep and extensive burns. Secretion of growth factors results in faster healing of donor sites and in better aesthetic results [3]. Developing new in vitro skin model would also allow avoiding tests on humans or animals. These skin substitutes also constitute much better models than artificial membranes to mimic normal human skin (NHS).

Skin consists in three principal layers: hypodermis, dermis and epidermis. Since the last decades, tissue engineering has been showing promising technical advances regarding the in vitro preparation of HSS. Production processes have been improved to obtain more complete substitutes, made of a dermis and an epidermis [3]. Most of the already commercialized bilamellar HSS consist of a matrix made of exogenous material (natural material, like collagen, or artificial material, like polymers) [3, 4]. The category of the bilayer skin substitutes includes six models characterized by the presence of autologous or allogeneic cells cultured with exogenous material to produce the dermal matrix. Some bilayer skin models are produced using autologous keratinocytes, seeded onto a dermal substitute made with autologous fibroblasts in a bovine collagen (PermaDerm™), hyaluronic acid ester (TissueTech™) or polymer (Polyactive) matrix. Other models as Apligraft® and OrCel® are produced with allogeneic human keratinocytes and fibroblasts, cultured in a bovine collagen sponge, while StrataGraft® is produced with allogeneic dermis and epidermis generated from a progenitor cell line: neonatal immortalized keratinocytes (NIKS®) [5, 6].

The self-assembly method, developed at the Laboratoire d'Organogenèse EXpérimentale (LOEX), allows the production of HSS without the need of any exogenous material. In fact, the self-assembly method does not need any scaffold to support the growing of the cells. Under specific culture conditions, the cells will produce their own extracellular matrix. The HSS consist of a dermis and an epidermis, the latter being constituted of the stratum corneum (SC) and living epidermis (LE). Using the self-assembly method, it is possible to produce both healthy and psoriatic HSS, depending on the cell types used during the production process [7, 8]. As human skin substitutes produced with the self-assembly method are composed of both dermis and epidermis, they can be included in the bilayer category. Human skin substitutes produced using the self-assembly method distinguish themselves from the other models mentioned above because: (1) they are produced with autologous cells and (2) they are completely free of exogenous biomaterials, thus eliminating risks of rejection, infection or immune reactions in clinical applications. However, the production is time-consuming. Consequently, commercially skin substitutes can be a good alternative in case of emergency applications. [5, 6]

The skin has a barrier function between the organism and the environment, thanks to the well-organized structure of the SC, the outermost layer of the skin [9]. In the SC, the cells are embedded in a lipid matrix. Lipids present in the SC are essentially fatty acids, ceramides and cholesterol [9-11]. The molecular organization provided by the tightly packed lipid bilayers [10, 12] ensures an efficient barrier function [13].

Percutaneous absorption was measured by the standard Franz diffusion cell technique. Even if the HSS show a similar absorption profile to NHS, few differences appear, probably due to the lack

of organization of the lipids [8]. The surfaces of these HSS have already been characterized using attenuated total reflectance infrared spectroscopy. Basically, this study demonstrated that the level of lipid order was lower in the HSS than in NHS [14]. Moreover, the three characteristic layers of the HSS (SC, LE and dermis) have been qualitatively studied using infrared microspectroscopy imaging, with focus on protein conformation and lipid distribution and organization [15].

Vibrational spectroscopies (infrared and Raman) are non-invasive and non-destructive optical techniques that can both provide direct molecular-level information on biological tissues. They do not require any special sample preparation or pre-treatment. These analytical methods are based on the detection of chemical group frequencies that are in turn, sensitive to molecule structure, organization, and conformation. Accordingly, both infrared and Raman spectroscopies have been previously demonstrated to be powerful complementary techniques for the determination of lipid organization and protein secondary structure. Some vibrational modes active in IR absorption are inactive in Raman scattering and vice versa. The IR stretching modes of methylene groups for instance are highly sensitive to the acyl chain order whereas the amide I band provides insight into the secondary structure of proteins. Moreover, sampling with a microscope coupled to an infrared (IR) spectrometer allows a rapid recording of images and their corresponding set of spectra at high signal-to-noise ratios. On the other hand, whereas Raman spectra exhibit similar informative vibrational modes, it also provides specific information about the carbon skeleton of lipid acyl chains and amino acid side chains. Raman has also a higher spatial resolution and can be used in confocal mode [13, 16-23].

The structure of NHS [23-28] and HSS [29, 30] have already been studied using Raman spectroscopy. In vivo confocal Raman spectroscopy has also been used to measure skin hydration and to monitor the penetration of active molecules through human skin [31-34]. The monitoring of the permeation of exogenous phospholipid vesicles applied topically to pigskin has been realized by combining both confocal Raman microspectroscopy and IR microspectroscopy imaging [35]. To our knowledge, the present study is the first to use Raman microspectroscopy to monitor the structure of HSS produced without any exogenous material, using the self-assembly method. In this paper, we report a comparative study between HSS produced using the self-assembly method, and NHS, using Raman microspectroscopy. This technique is well-known to allow an in-depth quantitative information on the characteristic layers of the HSS and NHS in terms of composition, lipid order and protein conformation. The ultimate aim is to prove that the HSS developed by the LOEX could be an adequate model of human skin.

2 MATERIALS AND METHODS

2.1 Patients

Dermal fibroblasts and dermal keratinocytes have been extracted from biopsies taken from breast reduction surgery. The subjects were females aged of 18 and 38 years (F18 and F38). Several biopsies taken from 44-years-old (NHSF44) and 48-years-old (NHSF48) women breast reduction surgeries were used as controls.

This study was conducted in agreement with the Helsinki declaration and performed under the guidelines of the research ethics committee of the ‘‘Centre Hospitalier Universitaire de Québec”. All patients were given adequate information to provide written consent.

2.2 Cell culture media

Fibroblasts were cultured in the Dulbecco-Vogt modification of Eagle’s medium (DMEM) supplemented with 10% fetal calf serum (Invitrogen, Burlington, Ontario, Canada), 100 UI.mL^{-1} penicillin G (Sigma, Oakville, Ontario, Canada) and 25 µg.mL^{-1} gentamicin (Schering, Pointe-Claire, Québec, Canada). Keratinocytes were cultured in a combination of DMEM with Ham’s F12 (3:1)

supplemented with 5% Fetal Clone II serum (Hyclone, Scarborough, Ontario, Canada), 5 $\mu g.mL^{-1}$ insulin (Sigma), 0.4 $\mu g.mL^{-1}$ hydrocortisone (Calbiochem, EMD Biosciences, Gibbstown, NJ, USA), 10-10 M cholera toxin (MP Biochemicals, Montréal, Québec, Canada), 10 $ng.mL^{-1}$ human epidermal growth factor (EGF) (Austral Biological, San Ramon, CA, USA), 100 $UI.mL^{-1}$ penicillin (Sigma) and 25 $\mu g.mL^{-1}$ gentamicin (Schering).

2.3 Production of human skin substitutes

HSS were produced using the self-assembly method developed at the LOEX, as previously described [15]. Briefly, human dermal fibroblasts were seeded in flasks and cultured with ascorbic acid at a concentration of 50 $mg.mL^{-1}$. After 28 days of culture, two manipulable dermal fibroblast sheets were superimposed to form a reconstructed dermis. These dermal substitutes were then incubated to insure the cohesion of the two sheets. After 7 days of incubation, the reconstructive dermises were seeded with human epidermal keratinocytes. After 7 days of culture immersion in DME-HAM with ascorbic acid, the substitutes were brought to the air-liquid interface. Differentiation was stopped after 21 days of culture. Biopsies of the substitutes were then embedded in Optimum Cutting Temperature compound (OCT, Tissue-Tek* O.C.T. Compound, Sakura* Finetek) and frozen for further analyses.

2.4 Histological analyses

Biopsies of the substitutes were fixed with Histochoice's solution and embedded in paraffin. Five micrometers thick sections were cut and stained using Masson's Trichrome. This allowed distinguishing the different layers of the HSS (SC, LE, and dermis).

2.5 Raman microspectroscopy

Controls and samples were cut in transverse 20 µm-thick sections. The cryotomed sections were put in place on glass microscope slides and then stored in the freezer at -20°C. All sections were then analyzed without any further modification.

Raman spectra were recorded using a LabRam HR-800 spectrometer (Horiba Jobin-Yvon, Villeneuve d'Ascq, France) coupled to an Olympus BX-30 fixed stage microscope, equipped with an open electrode Peltier-cooled CCD detector (1024x256 pixels) (Andor Technology, Belfast, Northern Ireland). A MPlan 100X objective (0.90 NA) (Olympus) was used for the data collection. An internal He-Ne laser set at 633 nm (red) was used for the acquisition of all the spectra. We used a 600 lines/mm grating. The confocal hole and the entrance slit of the monochromator were fixed at 400 µm and 100 µm, respectively. All spectra were the result of three acquisitions of 60 seconds each. The fingerprint region ranges from 700 to 1800 cm-1 while the high wavenumber region ranges from 2500 to 3200 cm^{-1}.

Ten spectra were taken in each characteristic layer of the skin substitute and NHS (SC, LE, and dermis) and were analyzed using GRAMS/AI 8.0 (ThermoGalactic, Salem, NH). A cubic function was used on each spectral region for the baseline correction to get rid of the scattering. All spectra were normalized according to different criteria as a function of the spectral feature of interest: in the fingerprint region, spectra were normalized with the amide I band (1650 cm^{-1}) intensity, while in the high frequency region, spectra were normalized using the intensity of the band located at 2930 cm^{-1}. The ten spectra were then averaged to obtain a unique spectrum per characteristic layer. Finally, the Fourier smoothing function of Grams was applied using a correction factor of 30%. This factor removes noise without significantly altering the shape of the bands.

For a given cell line, one or more section of 3 independently grown substitutes were analyzed (3 sections for F18-1, F18-2 and F18-3, 1 section for F38-1, F38-2, F38-3). For controls, four or more sections were analyzed (6 sections for NHS44F and 4 sections for NHS48F). Despite the natural

variability that occurs in HSS, the averaged spectra of a given layer are comparable for all the investigated substitutes: the wavenumber positions of the bands are comparable, and the trends observed are the same. Consequently, the results of only one representative HSS will be presented in order to simplify the presentation of the results. Accordingly, the depicted spectra originated from the HSS produced using cells taken from a biopsy of an 18 years old female (F18). For the control sample, the presented spectra are averaged from those recorded from six different sections.

3 RESULTS AND DISCUSSION

3.1 Macroscopic analyses

Figure 1 presents the macroscopic view of the HSS produced using the self-assembly method. The white ring is an anchorage used to manipulate the substitute during the production process. The full-thickness substitute (dermis + LE + SC) is mainly present in the middle of the ring (hole). As seen in this figure, the substitutes have a homogeneous and smooth surface. The white opalescent part confirms the presence of the SC.

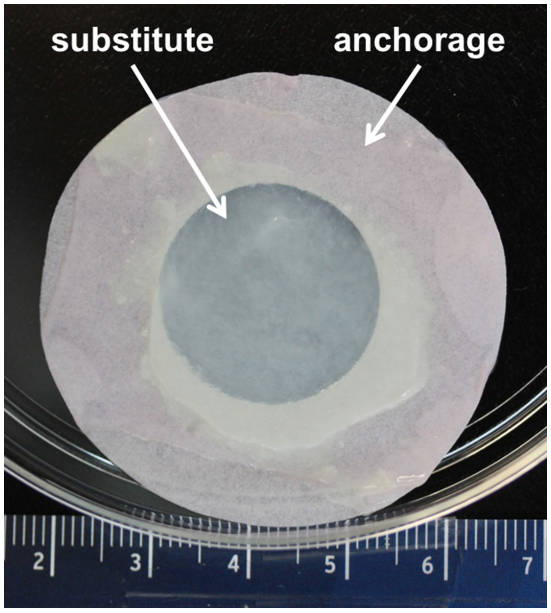

Figure 1. Macroscopic view of a human skin substitute produced using the self-assembly method (scale in centimeters)

3.2 Histological analyses

Masson's trichrome staining images of 5-µm thick biopsies show the structure of the HSS (Figure 2A). These histological analyses confirm that the self-assembly method allows to produce HSS with a structure resembling that of NHS. In fact, the characteristic skin layers are easily distinguishable with the dermis being identified by the presence of collagen fibers, appearing in light blue, and by the nuclei of the fibroblasts that are stained in purple. In addition, the cytoplasms of cells in the LE display a red color. Finally, basophilic substances found in the SC appear in dark blue. Compared to NHS (Figure 2B), the SC of the HSS is definitely thicker due to the absence of desquamation in vitro.

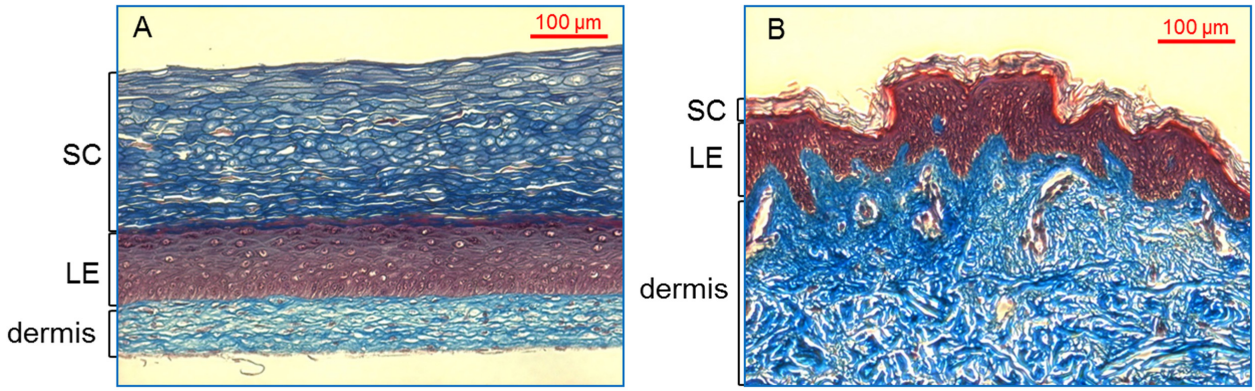

Figure 2. Histological images of (A) human skin substitute produced using the self-assembly method compared to (B) normal human skin (scale bar = 100 µm).

3.3 Comparison between lipid and protein in skin substitutes and NHS

Figure 3 shows a microscopic image of a section of an HSS. Even in the absence of staining, the three main layers are easily distinguishable (SC, LE, dermis). Dots on the image correspond to locations where the spectra were recorded (10 spectra per layer).

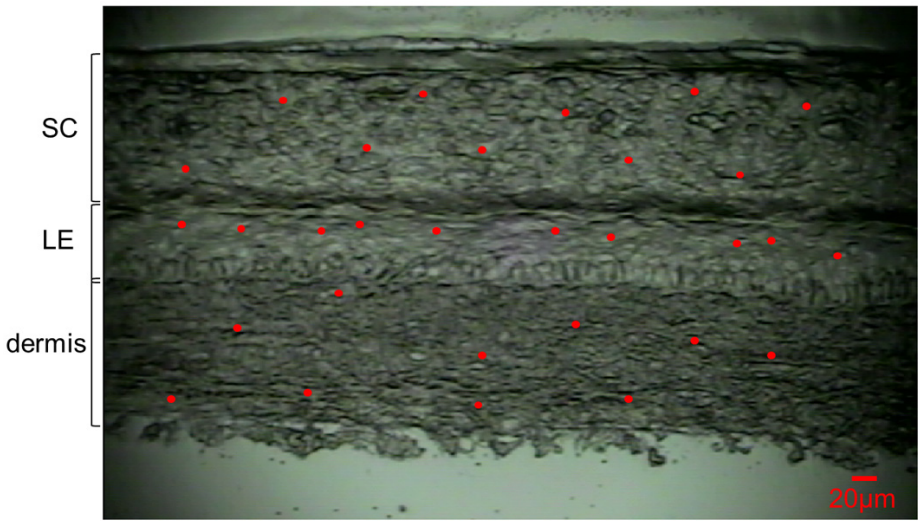

Figure 3. Microscopic image of a human skin substitute section (10X objective). Red dots correspond to places where the spectra have been taken to then be averaged (scale bar 20 µm).

Figure 4 displays superimpositions of the resulting Raman spectra of the SC, LE and dermis of HSS and NHS. Two spectral regions are of particular interest for characterizing lipid and protein-containing materials. As aforementioned, they are identified as the fingerprint region that is located between 700 and 1800 cm^{-1}, and the high frequency region, ranging between 2500 and 3200 cm^{-1}. These two regions exhibit spectral features assigned to both lipids and proteins. Table 1 summarizes the assignments of the bands that were identified in the spectra of the different layers (SC, LE, dermis) of the HSS. For each wavenumber, a description of the vibrational mode and an origin of the vibration are suggested on the basis of previously published literature.

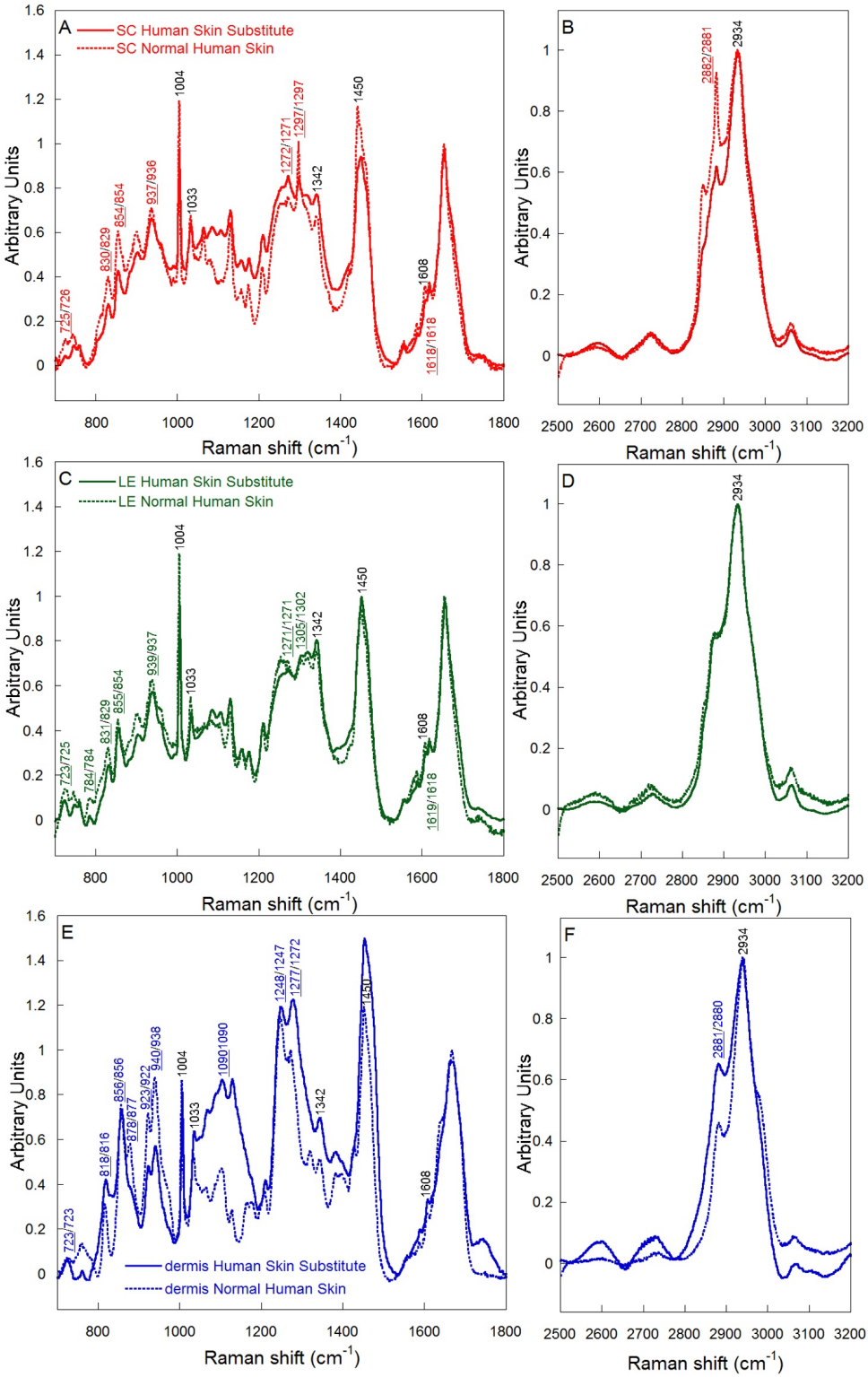

Figure 4. Resulting average Raman spectra of the (A and B) stratum corneum (SC), (C and D) living epidermis (LE) and (E and F) dermis of a human skin substitute (full lines) and normal human skin (dotted lines) showing the high frequency (2500 and 3200 cm-1) and the fingerprint regions (700 and 1800 cm-1). Common features to all layers are identified in black. Underlined frequencies refer to human skin substitute.

Table 1. Assignments of the Raman bands that are identified in the spectra of the different layers (stratum corneum (SC), living epidermis (LE), dermis) of the human skin substitute.

Wavenumber (cm^{-1})			Assignments and approximate description of vibrational modes	Component at the origin of vibration	Ref
SC	LE	Dermis			
	723	723	ρ(CH_2)	DNA	[17, 19, 27, 29]
725			υ(C-S) *trans*	Contribution: cysteine	[29]
X	784	shoulder	υ(C-C) (pyrimidine ring)	Nucleic acid Cytosine DNA	[17, 23, 28]
		818	υ(C-C)	Collagen backbone	[36, 37]
830	831		δ(C-CH) aliphatic	Tyrosine Fermi Doublet	[29, 36, 38]
854	855		δ(C-CH) aromatic	Tyrosine Fermi Doublet	[29, 36, 38]
		856	υ(C-C)	Proline ring collagen	[23, 28, 36, 37]
		878 (shoulder)	υ(C-C)	Hydroxyproline ring collagen	[23, 28, 36, 37]
		923	υ(C-C)	Collagen proline ring	[23, 28, 36, 37]
937	939		υ(C-C)	α-helix	[24, 27, 29, 39]
		940	υ(C-C)	Collagen backbone Gly-X-Y / proline ring	[23, 28, 36, 37]
1004	1005	1005	υ(C-C) aromatic symmetric ring breathing	Phenylalanine	[18, 21, 23, 29, 30, 40, 41]
1033	1034	1035	C-H in-plane bending	Phenylalanine	[29, 40]
1064	1067	1067	υ(C-C) skeletal, *trans* conformation	Mainly intercellular lipid alkyl chains with minor protein contribution	[18, 25, 28, 29, 39, 40]
1085	1086		υ(C-C) skeletal, *gauche* conformation	Mainly intercellular lipid alkyl chains with minor protein contribution	[18, 25, 28, 29, 39, 40]
		1090	Phosphodiester band of DNA		[22]
1106	1106		υ(C-C) *gauche* conformation	Lipids	[29]
1130	1129	1128	υ(C-C) skeletal, *trans* conformation	Mainly intercellular lipid alkyl chains with minor protein contribution	[18, 25, 28, 29, 39, 40]
1209	1210	1209	υ(C-C_6-H_5)	Phenylalanine	[29]
		1248	υ(CN) and δ(NH) amide III	Collagen: proline rich	[28, 29, 36, 37, 40, 42]
1272	1271	1277	υ(CN) and δ(NH) amide III	α-helix Collagen: proline poor	[24, 28, 29, 36, 37, 39, 40, 42]
1297	1305		δt(CH_2)	Lipids	[18, 23, 28, 29, 43]
1341	1341	1344	skeletal δ(CαH) + υ(CCα) + δ(NH)	Proteins	[44]
1450	1451	1453	δ(CH_2) scissoring δ(CH_2) and δ(CH_3)	Lipids Proteins	[18, 21, 27, 28, 40, 45]
1588	1588	1589	υ(C=C) olefinic	Proteins	[27, 40]
1608	1609	1608	C=C	Phenylalanine	[27, 46]
1618	1619		In plane ring stretching	Tyrosine	[27]

1654	1656	1667 (narrow)	υ(C=O) peptide bond amide I	Proteins 1655: α-helix 1660: random coil	[24, 27, 29, 36, 39, 40]
2852			$\upsilon(CH_2)$ symmetric	Essentially lipids	[28, 40]
2882	2877	2881	$\upsilon(CH_2)$ asymmetric	Mostly lipids with minor protein contribution	[28, 40]
2934	2933	2939	$\upsilon(CH_3)$ symmetric	Mostly proteins but with significant lipid contribution	[28, 40]
3063	3064	3065	υ(CH) olefinic	Predominantly proteins	[28, 40]

υ, stretch; δ, deformation; γt twisting; γ_w wagging

First, it can be noticed that some vibrational modes are present in the three layers of the HSS as well as in NHS. For example, the band at 1004 cm^{-1} corresponds to the C-C breathing vibrational mode of the benzene ring of the phenylalanine amino acid residue [18]. The intensity of this Raman band remains almost constant in the three layers of the substitutes and accordingly, this feature may be used as an internal standard [21, 23, 30, 41]. The presence of phenylalanine is also confirmed by the appearance of bands at 1608 and 1033 cm^{-1} arising from proteins (C=C stretch and C-C skeletal stretching, respectively) [40, 46].

The vibrational mode at 1342 cm^{-1} is also present in the three layers of the HSS and of NHS. It is characteristic of proteins and corresponds to CH_2 and CH_3 deformation [17, 28]. The vibrational mode at 2934 cm^{-1} is present in the three layers and is assigned to the CH3 stretching mode of proteins. The peak at 1451 cm^{-1} is assigned to the CH_2 and CH_3 deformations of proteins and lipids. This band is relatively conformation-insensitive and has been suggested as an intensity standard [18, 21, 45].

The three characteristic layers display different spectral features. The averaged spectrum of the SC of the HSS is characteristic of a lipid rich region. The weak peak at 1297 cm^{-1} arises from the CH_2 twisting mode of all-trans acyl chains as found in the ordered lipid lamellae of the SC [18, 23, 28]. The presence of lipids is also confirmed by the narrow band located at 2882 cm^{-1}, which is assigned to the CH_2 asymmetric stretching mode of acyl chains [40]. This information is consistent with the fact that the SC is well-known to be a lipid-rich layer, consisting of cells embedded in the lipid matrix. Compared to NHS, the vibrational band at 1297 cm^{-1} is less intense in the HSS, indicating that the amount of lipids is lower in the HSS than in NHS. Previous studies have reported the presence of droplets in the SC of the skin substitutes corresponding to an accumulation of triglycerides, resulting from major aberrations of carbohydrate-lipid metabolism, leading to an imbalance in synthesis of individual ceramide classes [47]. This is confirmed by the spectra in the high frequency region that show a strong and narrow band at 2881 cm^{-1} in NHS. The strong band at ~ 2933 cm^{-1} is characteristic of the CH stretching vibration of proteins and shows the strong contribution of protein molecules, especially in the dermis.

In the HSS, the averaged spectrum of the LE is globally quite similar to that of the SC. However, the lipid bands described above (1297 and 2882 cm^{-1}) are less intense. This means that the lipid content is lower in the LE than in the SC. Moreover, the peak at 1297 cm^{-1} is shifted to higher wavenumbers (1305 cm^{-1}), indicating more disordered lipid chains (i.e. a higher gauche conformer content) [43]. The presence of lipids is also confirmed by the vibrational features at 1067, 1086 and 1129 cm^{-1}, for which a more detailed analysis will be presented below. The characterization of the HSS by infrared microspectroscopy has already shown that there are fewer lipids in the LE [15]. Compared to NHS, the same decrease in lipid content and the same loss in lipid order are noticed here.

The spectrum of the dermis is very different from the spectra of the SC and of the LE. The dermis of the HSS is known to be a protein-rich region consisting of cells embedded in a protein matrix containing mainly collagen. In the dermis of HSS, some modes characteristic of collagen are present in the fingerprint region. A characteristic pair of doublets can be observed at 856/878 cm^{-1} and 923/940 cm^{-1} [23]. In fact, all of the collagen types consist of a set of three polypeptide chains called

tropocollagen, with each polypeptide chain being characterized by a Gly-X-Y sequence where X corresponds frequently to proline and Y to hydroxyproline [36]. Proline and hydroxyproline represent about one fourth of the amino acids in collagen [28]. Vibrational modes at 856, 923 and 940 cm^{-1} correspond to the C-C stretching of the proline ring, whereas the vibrational mode at 878 cm^{-1} corresponds to the C-C stretching of hydroxyproline ring [28, 36]. The band at 818 cm^{-1}, which is only present in the dermis, is assigned to the C-O-C stretching vibration and can be associated with the glucosyl-galactosylhydroxylysinonorleucine cross-linked between the tropocollagens. This spectral feature is correlated with the fibrillar structure of collagen I [36]. Because the dermis is rather poor in lipids, the 2881 cm^{-1} feature is assigned to CH_2 stretching mode of methylene moieties in lateral groups of proteins [40].

Pair of doublets at 856/877 cm^{-1} and 922/938 cm^{-1}, and the band at 816 cm^{-1} are also present in both NHS but the ratio of intensities of the bands are different. The dermis of the substitutes contains only one type of cell (fibroblasts) in extracellular matrix, whereas the dermis of NHS is a more complex layer which contains more cell types and structures in extracellular matrix. This explains the differences observed comparing the dermis of the substitutes with the dermis of NHS.

3.4. Comparison of skin substitute and NHS in terms of molecular and cellular organization

Several other vibrational modes are observed in the Raman spectra of HSS and NHS that allow characterizing molecular and cellular organization. For instance, the bands at 723 and 784 cm^{-1} are assigned to stretching vibration modes of DNA molecules in the cell nuclei [17, 19, 23, 27, 28]. Their simultaneous observation can be used to probe the presence of cells within the various layers of the skin samples. Indeed, the Raman spectra recorded from the LE of both the HSS and NHS clearly exhibit these two features, while the 784 cm^{-1} band is rather seen as a shoulder in the spectra of the dermis and is definitely absent for SC. This is consistent with the fact that, in the SC, corneocytes are known to be in their final differentiation state and do not have any nucleus components, and consequently, are devoid of DNA material. It is noteworthy that a component located at 725 cm^{-1} is also observed in the SC spectra without the 784 cm^{-1} band, which rules out an assignment to DNA. The assignment of this component is more consistent with cysteine residues that are abundant in keratin [29]. In the dermis, particularly, the vibrational mode at 1090 cm^{-1} may be assigned to the phosphodiester moiety of DNA [22]. The dermis contains a high density of cells embedded in the extracellular matrix, which explains the presence of the band at 1090 cm^{-1}.

The bands located near 830 and 854 cm^{-1} are well-known to be associated with aromatic ring vibrations of tyrosine residues and originate from Fermi resonance interactions [38]. These two peaks are present only in the SC and in the LE and are absent in the dermis. The band at 1618 cm^{-1}, present in the SC, in the LE, and overlapped in the dermis, confirms the attribution of this doublet to tyrosine side-chain vibrations [27]. This doublet has been found to be sensitive to the environment of the tyrosine residues. The intensity ratio I_{854}/I_{830} is related to the environment of the phenolic hydroxyl group of tyrosine residues (exposed or buried). When the higher frequency peak is stronger, the tyrosyl residues are exposed inducing intermolecular bonding. When the lower frequency peak is stronger, the tyrosine residues are buried within the protein (mainly in hydrophobic region), inducing intramolecular bonding [29, 36, 38]. In the SC and in the LE, the intensity of the vibrational mode located near 854 cm^{-1} is higher than the one at 830 cm^{-1} indicating that the tyrosyl residues are mainly exposed for both the NHS and substitute.

Figure 5 displays the superimposition of averaged spectra from the SC and the LE, in the frequency domain ranging from 1000 to 1150 cm^{-1}. This domain is particularly relevant to study the lipid order of the skin layers. Indeed, the vibrational modes at 1064 and 1130 cm^{-1} correspond to the C-C skeletal stretching vibration of lipids in trans conformation (ordered phase), whereas the vibrational mode at 1085 cm-1 correspond to the C-C skeletal stretching vibration of lipids in gauche conformation (disordered phase) [18, 25, 28, 29, 39, 40]. The lipid packing can thus be semi-quantitatively evaluated using the intensities of the peaks at 1064 and 1130 cm^{-1} when compared

with the intensity of the band at 1085 cm^{-1} (intensity ratios I_{1064}/I_{1085} and I_{1130}/I_{1085}). The lower the ratios, the higher the gauche conformer content and the more disordered the lipid chains. Histograms in Figure 5 show these ratios for various samples in the SC and LE of NHS and HSS. One can observe a decrease of both ratios between the SC and the LE, indicating a decrease in lipid order from the SC to the LE for both the HSS and NHS. It can also be concluded that the LE of both NHS and the HSS display a very similar lipid chain order while the lipids in SC of NHS are clearly more ordered than in the substitutes.

It should be emphasized that Raman spectroscopy does not allow a definitive determination of the lipid composition. As previously demonstrated, lipids in the LE of NHS are enzymatically modified at the junction with the SC [9, 48]. Therefore, this lipid composition change from the LE to SC was shown to influence the lipid chain order, which is more important in the SC than in LE as previously demonstrated by FTIR [49]. Moreover, in the LE (stratum granulosum), lipids are organized as double-wall vesicles. These vesicles flatten in the LE and fuse to form lipids bilayers in the SC [10]. Consequently, such a mechanism leads to an increase in the lipid order in the SC with respect to the LE. The steps involved in lipid bilayer formation could also be at the origin of the lipid order profile observed from the SC to the LE.

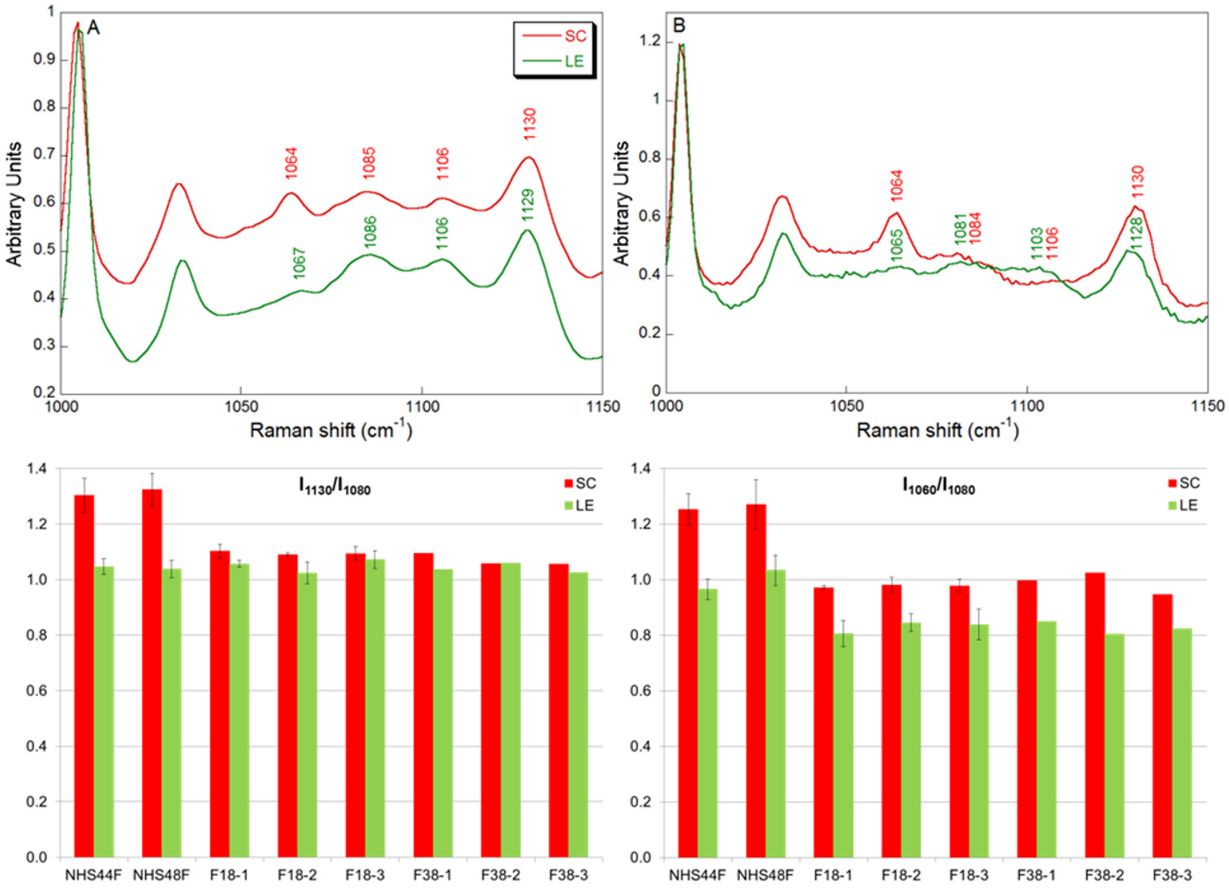

Figure 5. Raman spectra of the stratum corneum (SC, red) and living epidermis (LE, green) in the spectral region between 1000 and 1150 cm^{-1} for (A) human skin substitute and (B) normal human skin. (C) Histograms of the I1064/I1085 and (D) I_{1130}/I_{1085} ratios

Figure 6 displays the superimposition of averaged spectra from the SC, the LE and the dermis, in the amide I region. The amide I band originates mainly from the C=O stretching mode of the peptide bond [40] and gives useful information on the secondary structure of proteins. The

wavenumber of the maximum intensity, as well as the general line shape allows access to the secondary structure of proteins present in the different layers of the substitutes and NHS.

The narrow amide I band centered at 1654 cm^{-1} and 1656 cm^{-1}, in the SC and in the LE of the HSS, respectively, is characteristic of α-helix. The presence of a predominant α-helical structure is confirmed by the amide III band centered at 1272 cm^{-1} in the SC and 1271 cm^{-1} in the LE, and also by the presence of the peak at 938 cm^{-1} (Figure 4) [24, 27, 29, 39]. The presence of α-helices is consistent with the fact that the corneocytes in the SC are filled with keratin filaments whose conformation is α-helix. Keratin is also the most abundant protein in the LE and tends to progressively organize itself from the dermo-epidermal junction to the SC [18, 28, 40]. Moreover, another structure, most probably random coil or turns, is also present as shown by the shoulder near 1660 cm-1. It is remarkable that the shape and position of the amide I bands of SC and LE are nearly identical, which shows that the proteins constituting the SC and LE of the substitutes adopt the same predominant α-helix conformation as in the NHS.

In the dermis of the HSS, the amide I band is located at higher wavenumbers (1667 cm^{-1}) and is broader which can be attributed to the presence of type I collagen [36]. The shape of the amide III doublet at 1248 and 1277 cm^{-1} associated with proline-rich and proline-poor regions, respectively, is characteristic of the type I collagen and confirms that information [28, 36, 37, 42]. Other spectral contributions arising as shoulders at 1625 and 1690 cm^{-1} may be due to turns and/or disordered structures. The amide I band of the dermis of the HSS shares very similar features with those of the NHS: maximum of the amide I band near 1668 cm^{-1}, shoulder at 1625 and 1690 cm^{-1}. This spectral similarity suggests that the protein conformation of the HSS is close to that of NHS. However, some differences can also be noticed such as the broadening of the upper part of the spectrum which indicates a small conformational disparity. As already mentioned, the dermis of the substitute consists of fibroblasts embedded in an extracellular matrix containing mainly type I collagen [25, 28, 36], but the dermis of NHS contains more components than the dermis of the HSS which could explain the differences observed in the amide I and amide III regions.

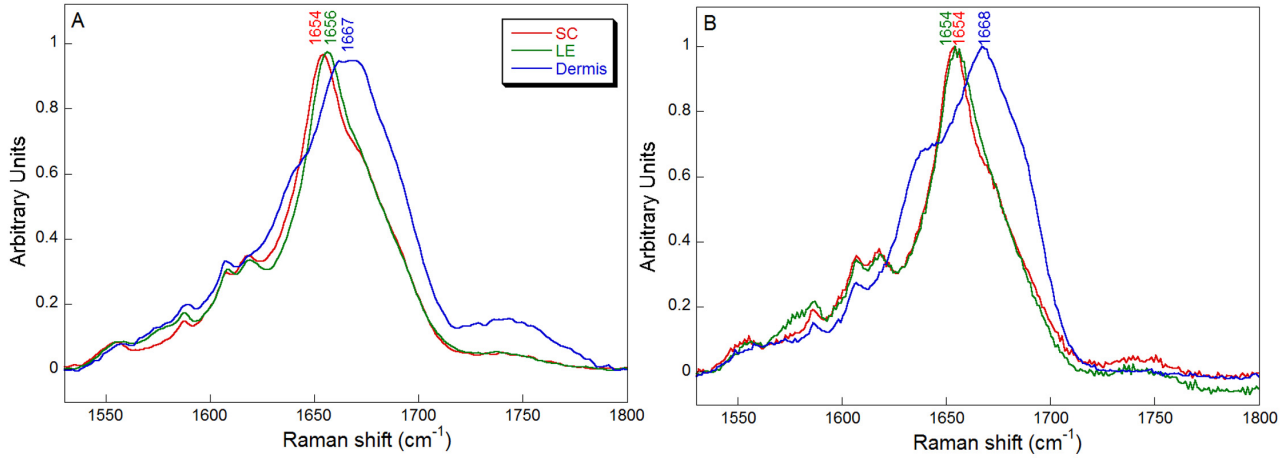

Figure 6. Superposition of averaged spectra from the stratum corneum (SC, red), the living epidermis (LE, green) and the dermis (blue), in the amide I region.

4 CONCLUSIONS

This study showed that Raman microspectroscopy is a powerful technique to characterize biomaterials like human skin substitutes. In fact, this technique allowed collecting data at a molecular level. Our results showed that human skin substitutes are similar to NHS in terms of protein secondary structure and lipid organization. Concerning lipids, we showed that, in both human skin substitutes and NHS, the SC is a lipid-rich layer, and that the lipids are more organized in the SC

than in the LE. However, the amount of lipids is higher, and the lipids contain more trans conformers in NHS compared to the substitutes. Concerning proteins, our results showed the predominance of α-helices in the LE and SC, which is consistent with the presence of keratin. The spectra in the dermis are characteristic of type I collagen which is the main constituent of the extracellular matrix. In view of these results the human skin substitutes produced using the self-assembly method could be considered as a promising human skin model.

ACKNOWLEDGEMENTS

The authors acknowledge the financial support from the Natural Sciences and Engineering Research Council of Canada (NSERC) and the Canadian Institutes for Health Research (CIHR) through their joint Collaborative Health Research program. The authors also thank Émile Robert, Marc-André Breton and Laurie Bédard for their contribution in this research, Jean-Francois Rioux-Dubé for his technical support and Michel Pézolet for helpful discussions.

REFERENCES

[1] WHO. Burns Fact sheet N°365. 2012.
[2] European Parliament C. Regulation (EC) No 1223/2009 of the European Parliament and of the Council of 30 November 2009 on cosmetic products (Text with EEA relevance). 2009.
[3] Auxenfans C, Fradette J, Lequeux C, Germain L, Kinikoglu B, Bechetoille N, et al. Evolution of three dimensional skin equivalent models reconstructed in vitro by tissue engineering. Eur J Dermatol 2009;19:107-13.
[4] Supp DM, Boyce ST. Engineered skin substitutes: practices and potentials. Clinics Dermatol 2005;23:403-12.
[5] Jean J, Garcia-Perez, ME., Pouliot, R. Bioengineered skin: the self-assembly approach. J Tissue Sci Eng 2011;S:5.
[6] Pouliot R, Larouche D, Auger FA, Juhasz J, Xu W, Li H, et al. Reconstructed human skin produced in vitro and grafted on athymic mice. Transplantation 2002;73:1751-7.
[7] Jean J, Lapointe M, Soucy J, Pouliot R. Development of an in vitro psoriatic skin model by tissue engineering. J Dermatol Sci 2009;53:19-25.
[8] Jean J, Leroy, M., Duque-Fernandez, A., Bernard, G., Soucy, J., Pouliot, R. Characterization of a psoriatic skin model produced with involved or uninvolved cells. J Tissue Eng Regen Med 2012:in press.
[9] Proksch E, Brandner JM, Jensen JM. The skin: an indispensable barrier. Exp Dermatol 2008;17:1063-72.
[10] Downing DT. Lipid and protein structures in the permeability barrier of mammalian epidermis. J Lipid Res 1992;33:301-13.
[11] Mizutani Y, Mitsutake S, Tsuji K, Kihara A, Igarashi Y. Ceramide biosynthesis in keratinocyte and its role in skin function. Biochimie 2009;91:784-90.
[12] Forster T. Cosmetic lipids and the skin barrier: CRC Press; 1 edition (December 19, 2001); 2001.
[13] Mendelsohn R, Flach CR, Moore DJ. Determination of molecular conformation and permeation in skin via IR spectroscopy, microscopy, and imaging. Biochim Biophys Acta 2006;1758:923-33.
[14] Bernard G, Auger M, Soucy J, Pouliot R. Physical characterization of the stratum corneum of an in vitro psoriatic skin model by ATR-FTIR and Raman spectroscopies. Biochim Biophys Acta 2007;1770:1317-23.
[15] Leroy M, Lafleur M, Auger M, Laroche G, Pouliot R. Characterization of the structure of human skin substitutes by infrared microspectroscopy. Anal Bioanal Chem 2013.

[16] Zhang X, Roeffaers MBJ, Basu S, Daniele JR, Fu D, Freudiger CW, et al. Label-free live-cell imaging of nucleic acids using stimulated Raman scattering microscopy. Chem Phys Chem 2012;13:1054-9.
[17] Movasaghi Z, Rehman S, Rehman IU. Raman spectroscopy of biological tissues. Appl Spectrosc Rev 2007;42:493-541.
[18] Huang Z, Zeng H, MacAulay CE, Hamzavi I, McLean DI, Lui H. Evaluation of variations of biomolecular constituents in human skin in vivo by near-infrared Raman spectroscopy. In: Jacques AETCHPSL, editor. Biophotonics Instrumentation and Analysis. Singapore, Singapore: SPIE; 2001. p. 109-14.
[19] Wang H, Lee AMD, Lui H, McLean DI, Zeng H. A method for accurate in vivo micro-Raman spectroscopic measurements under guidance of advanced microscopy imaging. Sci Rep 2013;3.
[20] Jell G, Swai, R., Stevens, M.M. Raman spectroscopy a tool for tissue engineering. In: Matousek P, Morris, M.D., editor. Emerging Raman applications and techniques in biomedical and pharmaceutical fields: Springer Berlin Heidelberg; 2010. p. 419-37.
[21] Zhao JH, Lui H, McLean D, Zeng HS. Real-time raman spectroscopy for noninvasive in vivo skin analysis and diagnosis. In: Campolo D, editor. New developments in biomedical engineering2010. p. 455-74.
[22] Zhang G, Moore DJ, Flach CR, Mendelsohn R. Vibrational microscopy and imaging of skin: from single cells to intact tissue. Anal Bioanal Chem 2007;387:1591-9.
[23] Flach CR, Moore DJ. Infrared and Raman imaging spectroscopy of ex vivo skin. Int J Cosmetic Sci 2013;35:125-35.
[24] Chrit L, Hadjur C, Morel S, Sockalingum G, Lebourdon G, Leroy F, et al. In vivo chemical investigation of human skin using a confocal Raman fiber optic microprobe. J Biomed Optics 2005;10:044007-.
[25] Caspers PJ, Lucassen GW, Wolthuis R, Bruining HA, Puppels GJ. In vitro and in vivo Raman spectroscopy of human skin. Biospectroscopy 1998;4:S31-S9.
[26] Caspers PJ, Lucassen GW, Puppels GJ. Combined in vivo confocal Raman spectroscopy and confocal microscopy of human skin. Biophys J 2003;85:572-80.
[27] Tfaili S, Gobinet C, Josse G, Angiboust JF, Manfait M, Piot O. Confocal Raman microspectroscopy for skin characterization: a comparative study between human skin and pig skin. Analyst 2012;137:3673-82.
[28] Ali SM, Bonnier F, Tfayli A, Lambkin H, Flynn K, McDonagh V, et al. Raman spectroscopic analysis of human skin tissue sections ex-vivo: evaluation of the effects of tissue processing and dewaxing. J Biomed Optics 2012;18:061202-.
[29] Tfayli A, Piot O, Draux F, Pitre F, Manfait M. Molecular characterization of reconstructed skin model by Raman microspectroscopy: comparison with excised human skin. Biopolymers 2007;87:261-74.
[30] Yu G, Zhang G, Flach CR, Mendelsohn R. Vibrational spectroscopy and microscopic imaging: novel approaches for comparing barrier physical properties in native and human skin equivalents. J of Biomed Optics 2012;18:061207-.
[31] Caspers PJ, Lucassen GW, Bruining HA, Puppels GJ. Automated depth-scanning confocal Raman microspectrometer for rapid in vivo determination of water concentration profiles in human skin. J Raman Spectrosc 2000;31:813-8.
[32] Pudney PDA, Melot M, Caspers PJ, van der Pol A, Puppels GJ. An in vivo confocal Raman study of the delivery of trans-retinol to the skin. Appl Spectrosc 2007;61:804-11.
[33] Caspers PJ, Lucassen GW, Carter EA, Bruining HA, Puppels GJ. In vivo confocal Raman microspectroscopy of the skin: noninvasive determination of molecular concentration profiles. J Invest Dermatol 2001;116:434-42.
[34] Caspers PJ, Williams AC, Carter EA, Edwards HG, Barry BW, Bruining HA, et al. Monitoring the penetration enhancer dimethyl sulfoxide in human stratum corneum in vivo by confocal Raman spectroscopy. Pharm Res 2002;19:1577-80.

[35] Xiao CH, Moore DJ, Rerek ME, Flach CR, Mendelsohn R. Feasibility of tracking phospholipid permeation into skin using infrared and Raman microscopic imaging. J Invest Dermatol 2005;124:622-32.
[36] Nguyen TT, Gobinet C, Feru J, Brassart-Pasco S, Manfait M, Piot O. Characterization of type I and IV collagens by Raman microspectroscopy: identification of spectral markers of the dermo-epidermal junction. Spectrosc-Int J 2012;27:421-7.
[37] Hwang YJ, Lyubovitsky JG. The structural analysis of three-dimensional fibrous collagen hydrogels by raman microspectroscopy. Biopolymers 2013;99:349-56.
[38] Siamwiza MN, Lord RC, Chen MC, Takamatsu T, Harada I, Matsuura H, et al. Interpretation of doublet at 850 and 830 cm-1 in Raman-spectra of tyrosyl residues in proteins and certain model compounds. Biochemistry 1975;14:4870-6.
[39] Barry BW, Edwards HGM, Williams AC. Fourier-transform Raman and infrared vibrational study of human skin - assignment of spectral bands. J Raman Spectrosc 1992;23:641-5.
[40] Anigbogu ANC, Williams AC, Barry BW, Edwards HGM. Fourier-transform Raman-spectroscopy of interactions between the penetration enhancer dimethyl sulfoxide and human stratum corneum. Int J Pharm 1995;125:265-82.
[41] Lo WL, Lai JY, Feinberg SE, Izumi K, Kao SY, Chang CS, et al. Raman spectroscopy monitoring of the cellular activities of a tissue-engineered ex vivo produced oral mucosal equivalent. J Raman Spectrosc 2011;42:174-8.
[42] Bonifacio A, Sergo V. Effects of sample orientation in Raman microspectroscopy of collagen fibers and their impact on the interpretation of the amide III band. Vibr Spectrosc 2010;53:314-7.
[43] Tfayli A, Guillard E, Manfait M, Baillet-Guffroy A. Thermal dependence of Raman descriptors of ceramides. Part I: effect of double bonds in hydrocarbon chains. Anal Bioanal Chem 2010;397:1281-96.
[44] Krimm S, Bandekar J. Vibrational Spectroscopy and Conformation of Peptides, Polypeptides, and Proteins. In: C.B. Anfinsen JTE, Frederic MR, editors. Advances in Protein Chemistry: Academic Press; 1986. p. 181-364.
[45] Mahadevan-Jansen A, Richards-Kortum RR. Raman spectroscopy for the detection of cancers and precancers. J Biomed Optics 1996;1:31-70.
[46] Lee HI, Kim MS, Suh SW. Raman-spectroscopy of L-phenylalanine, L-tyrosine, and their peptides absorbed on silver surface. B Kor Chem Soc 1988;9:218-23.
[47] Auger FA, Pouliot R, Tremblay N, Guignard R, Noel P, Juhasz J, et al. Multistep production of bioengineered skin substitutes: Sequential modulation of culture conditions. In Vitro Cell Dev-An 2000;36:96-103.
[48] Bouwstra JA, Honeywell-Nguyen PL, Gooris GS, Ponec M. Structure of the skin barrier and its modulation by vesicular formulations. Prog Lipid Res 2003;42:1-36.
[49] Lafleur M. Phase behaviour of model stratum corneum lipid mixtures: an infrared spectroscopy investigation. Can J Chem 1998;76:1501-11.